Journal of Chromatography A 1768 (2026) 466709

Contents lists available at ScienceDirect

Journal of Chromatography A

journal homepage: www.elsevier.com/locate/chroma

Screening terpene-based eutectic solvents for bisphenol A extraction from plastic-packed dairy products and water storage tanks: COSMO-RS and quantum chemistry calculations

Nazir Fattahi [a,1], Parvin Zohrabi [a,1], Pouya Karimi [b], Filipe Hobi Bordón Sosa [c], Beshare Hashemi [d,*], Fereshteh Shiri [b,e,*]

[a] Research Center for Environmental Determinants of Health (RCEDH), Health Institute, Kermanshah University of Medical Sciences, Kermanshah, Iran
[b] Department of Chemistry, Faculty of Science, University of Zabol, Zabol, Iran
[c] CICECO-Aveiro Institute of Materials, Chemistry Department, University of Aveiro, Aveiro, Portugal
[d] Department of Chemistry, Razi University, Kermanshah, Iran
[e] Informatics and Artificial Intelligence Research Center, Central Laboratory, University of Zabol, Zabol, Iran

ARTICLE INFO

Keywords:
Hydrophobic eutectic solvents
COSMO-RS
Quantum mechanical calculations
Bisphenol A

ABSTRACT

Bisphenol A (BPA) is globally used in the plastic and polymer industries. Regarding its toxicity, it raises health and environmental concerns due to its potential leaching into water, soil, and food chains. This work aims to screen the most efficient terpene-based hydrophobic eutectic solvents (HESs) for the extraction of BPA using COSMO-RS, an in-silico predictive approach, thereby minimizing the need for extensive trial-and-error experimentation. We also evaluated the extraction efficiency of HESs by assessing the stability of hydrogen bonding using quantum chemistry calculations. A HES composed of menthol: octanoic acid (2:1) was found to be the most efficient solvent after experimental validations. Experimental design showed the optimal extraction conditions to be 95 μL of menthol: octanoic acid (2:1), 100 μL of KOH 4.5 M, and 100 μL of HCl 5.0 M. A maximum extraction recovery of 75% with a limit of detection of 0.05 μg/L was achieved under the optimal extraction conditions in a pH-switchable extraction process. The environmental impact and applicability of the method were subsequently evaluated using AGREE, AGREEprep, and the blue applicability grade index, scoring 0.61, 0.66, and 65.0, respectively.

1. Introduction

Despite their low concentration, micropollutants have become a recent significant concern originating from pesticides, pharmaceuticals, plasticizers, and personal care products. Bisphenol A (BPA) is a widely used chemical in the plastic industry that has emerged as a micropollutant entering aquatic environments, raising public concern [1]. The United States Environmental Protection Agency set a critical limit of 50 μg/Kg for BPA in the human body [2]. Prolonged exposure to low concentrations of BPA via water and food sources can pose health risks. As an endocrine disruptor, BPA can damage the immune and reproductive systems [3]. Additionally, several health issues, including diabetes, obesity, and heart disease, are associated with BPA [4,5].

Given these harmful effects, the development of effective and sustainable sample preparation methods, such as solid-phase extraction and solvent-based extraction techniques, is mandatory. However, the demand for multiple preparation steps, consumption of conventional organic solvents, synthesis, and modification of solid phase led to the emergence of more sustainable and miniaturized methods adhering more to the principles of Green Chemistry [6].

Among various preparation techniques reported for the extraction of BPA [7–11], liquid-liquid microextraction (LLME) has grabbed notable attention owing to its distinguished advantages, including a simple and rapid extraction procedure, low solvent consumption, and reduced waste generation [6,12]. Furthermore, innovative extraction solvents enable the development of more sustainable liquid-phase microextraction methods.

Eutectic solvents (ESs) are a novel class of sustainable solvents

* Corresponding authors.
E-mail addresses: beshare.hashemi@gmail.com (B. Hashemi), fereshteh.shiri@gmail.com (F. Shiri).
[1] These authors are considered co-first authors because they contributed equally to this work.

https://doi.org/10.1016/j.chroma.2026.466709
Received 29 October 2025; Received in revised form 6 January 2026; Accepted 13 January 2026
Available online 15 January 2026

formed by mixing at least two components, typically a hydrogen bond acceptor (HBA) and a hydrogen bond donor (HBD). Through specific intermolecular interactions, mainly hydrogen bonding (HB), these mixtures exhibit a pronounced melting point depression compared to their pure constituents, leading to the formation of a liquid at or near room temperature. The careful selection of HBA and HBD enables the design of more sustainable ESs for a specific application [13]. Deep eutectic solvents (DESs) are ESs that reveal a notable negative deviation from ideality due to the solid-liquid equilibrium formation between a HBA and HBD. The deep depression in the melting temperature of a DES is attributed to stronger intermolecular interactions in the solvent compared to those in the parent precursors [13,14].

Depending on the specific HBA and HBD used, ESs can be either miscible or immiscible with water. Very recently, our research group employed hydrophobic ESs (HESs) to extract mainly environmental contaminants from various real samples, including vegetables, personal care products, and water samples, addressing the main concern related to the leachability of the ESs [15–18]. In all reported studies, HESs were formed by mixing low-solubility HBAs and HBDs. The hydrophobicity of the solvent was then converted by adjusting the acidity of the solution.

So far, various HESs have been employed to extract BPA from different matrices. For example, Ferreira et al. [19] prepared three menthol (Ment)-based HESs in combination with acetic acid (AcetA), decanoic acid (DecA), and dodecanoic acid (DoDecA) for the extraction of BPA from sludge samples. Among the tested HESs, Ment: AcetA was selected due to its lower viscosity, which made it more compatible with the pyrolizer for GC–MS analysis. Although AcetA exhibited a lower logP (−0.28), it was selected as HBA to prevent overlapping between the HES retention time and that of the analyte. Similarly, Cao et al. [20] used thymol (Thym) as an HBA paired with a range of carboxylic acids to extract BPA from water samples, achieving a high extraction efficiency (81 %) with DoDecA as the HBD. In another study, Rodríguez-Llorente et al. [8] applied the conductor-like screening model for real solvents (COSMO-RS) to identify the most suitable HES among forty-three candidates. Despite their simplicity and high extraction efficiency, these studies only evaluated the BPA extraction from water, which represents a relatively simple matrix.

The primary aim of this work is to develop a simple yet effective LLME method that exploits the phase conversion behavior of HESs. To this end, we designed diverse HESs composed of Ment and Thym as HBAs combined with two different carboxylic acids and alcohols, including octanoic acid (OctA), DecA, octanol (OctOl), and decanol (DecOl) as HBDs. Ment and Thym were selected in this work due to their hydrophobicity, hydrogen bonding capability, and environmental compatibility, which make them suitable components for the design of HESs. In addition, their hydrophobic, bulky framework and the presence of hydroxyl groups provide favorable van der Waals interactions with BPA and enable participation in HB formation. Compared to other natural components, such as polyols, sugars, and amino acids, terpenes exhibit lower water solubility and facilitate rapid phase separation. Unlike previous studies that restricted their evaluations to BPA extraction from water as a simple matrix, our approach is extended to more complex matrices, including yogurt and milk, in addition to 120 real water samples. Following the COSMO-RS and experimental extraction recoveries, the most efficient HESs were selected. Additionally, we investigated the stability of the selected HESs and the HB interactions using quantum chemistry calculations. Subsequently, to achieve the maximum extraction yield for the most effective HES, different variables, namely solvent volume, base concentration, and acid volume, were investigated using central composite design (CCD). This integrated experimental-computational strategy provides deeper insight into the HES-analyte interactions, demonstrating the applicability of the developed approach to both aqueous and dairy matrices, thus broadening the practical relevance of this sustainable extraction method.

2. Materials and methods

2.1. Chemicals and instrumentation

BPA and all parent components necessary for preparing the HESs, including Ment, Thym, OctA, DecA, OctOl, and DecOl were purchased from Sigma-Aldrich. HCl, KOH, and HPLC eluents were supplied by Merck. All the reagents were analytical grade, with purity greater than 97 %.

Water samples were collected from twenty garden house units, twenty apartment units, and twenty villa units. From each unit, ten plastic and metallic water storage tanks were selected for sampling. Half of the tanks were in the shaded areas or the basement, while the other half were on the roofs, exposed to the sunlight. A total of 120 samples were collected from the water tanks during the summer and winter seasons. All the samples were kept at 4 °C in glass bottles to eliminate the risk of BPA leaching during the sampling and pre-analysis stage.

All dairy products were obtained from local supermarkets in Kermanshah, Iran. To prepare milk, cocoa milk, and coffee milk samples, 5 mL of each was first filtered through a 0.2 μm syringe filter. Then, 1 mL $ZnSO_4$ (30 % w/v) was added, and the mixture was vortexed for 3 min. The mixture was subsequently centrifuged at 2795 g for 4 min. The supernatant was transferred to a clean sample tube and diluted to 10 mL with deionized water. For the yogurt sample, 2 g was accurately weighed and transferred to a clean sample tube. The sample was homogenized with 2 mL of water using a vortex mixer for 1 min, followed by the same procedure applied to other dairy products.

To analyze BPA, an HPLC-UV system (Knauer, Germany) was employed. An HS-ODS C18 column (15 cm × 4.6 mm, with a particle size of 5 μm) from Anachem (Luton, UK) was used for the separation of BPA. The chromatographic analysis was performed in an isocratic mode using 45:55 water: acetonitrile at a 1 mL/min flow rate. The instrument was equipped with a 20 μL manual injection loop (model 7725i, Rheodyne, Cotati, CA, USA), and the detector was set at 225 nm for the determination of BPA, which exhibited a retention time of 5.23 min. To minimize carry-over effect, particularly after the injection of high-concentration extracts, the HPLC system was thoroughly rinsed with acetonitrile for 5 min at a 1 mL/min flow rate. The system was then re-equilibrated with the mobile phase before subsequent injections. Blank solvent injections were performed intermittently to verify the absence of analyte and solvent residue in the chromatographic system.

2.2. Computational methods

COSMO-RS was employed to evaluate the ability of the designed HESs to interact with and dissolve BPA based on the calculation of the activity coefficient at infinite dilution at 298.15 K. To accomplish this, the charge distribution and the molecular geometry of all components were calculated and optimized using Turbomole v4.5.2, with BP86/TZVP level [21].

All quantum mechanical (QM) calculations were performed at the B3LYP/6–31+*G*(d,p) level of theory using the Gaussian09 software package [22] . The wave functions corresponding to geometries were analyzed using the quantum theory of atoms in molecules (QTAIM) with AIM2000 software [23]. Charge displacement (CD) curves were generated using the wave functions obtained by AIM2000.

Response surface methodology (RSM), a widely used optimization approach, was utilized to evaluate the effects and interactions of multiple variables on the extraction efficiency of the proposed method. To achieve this, a CCD was used at five levels to investigate the optimum extraction conditions that lead to the maximum extraction efficiency. The HES volume (X_1), KOH concentration (X_2), and HCl volume (X_3) were selected as independent variables affecting the extraction efficiency, as shown in Table 1. Eighteen experimental runs were generated by CCD, and the extraction recovery (ER %) of BPA was collected as the dependent variable, as reported in Table S1. The collected results were

Table 1
Coded levels used in CCD.

Independent variables	Symbol	Coded levels				
		-α	−1	0	+1	+α
HES volume (μL)	X_1	50	70	100	130	150
KOH concentration (M)	X_2	3	4	5	6	7
HCl volume (μL)	X_3	100	110	125	140	150

then analyzed by Design-Expert v10 statistical software (Stat-Ease, Minneapolis, USA). The statistical significance of the regression coefficients was evaluated using ANOVA, including an F-test at a 95 % confidence level. The adequacy of the fitted quadratic model was assessed by examining the coefficient of determination (R^2) and conducting a lack-of-fit test.

2.3. HESs preparation

HESs were prepared by mixing the respective pairs of HBAs/HBDs in varying compositions. The mixtures were heated at 50–80 °C and stirred at 2795 g until a clear, homogenous liquid was obtained.

3. Results and discussion

Activity coefficient at infinite dilution (γ^{∞}) provides an insight into the solubility of a solute in a given solvent and can be used as a potential criterion for selecting the most suitable compositions for experimental preparation. For ideal solutions, γ^{∞} approaches one, whereas it deviates from unity in non-ideal solutions [8]. COSMO-RS was used to calculate γ^{∞} of BPA in various HESs composed of Thym, Ment, OctA, DecA, OctOl, and DecOl. A lower value of ln γ^{∞} indicates stronger interactions between the solute and the solvent, corresponding to a higher thermodynamic tendency of the solute to dissolve in that solvent.

The results presented in Fig. 1 show that Thym-based mixtures yielded higher ln γ^{∞} values for BPA compared to Ment-based mixtures, suggesting that BPA interacts less favourably with Thym-based solvents. In addition, DecA and DecOl resulted in higher γ^{∞} in both groups of the HESs due to their increased hydrophobicity. In contrast, the shorter alkyl chain in acid or alcohol allows for better solvation of BPA, facilitating solute-solvent interactions.

Furthermore, the low solubility of BPA in Ment: Thym can be attributed to the similar structure of HBA and HBD, which limits the synergistic effects of the mixture. The 1:1 mixture is close to ideal, and the balanced network, along with the strong interaction between the HBA and HBD, might reduce the solvent's ability to interact with BPA. The higher solubility observed in the 2:1 Ment: Thym composition can be linked to the excess Ment, which promotes stronger hydrogen bond interactions and creates a more favorable solvent environment for BPA.

The excess enthalpy of mixing (H^E) was also evaluated using COSMO-RS to understand the intermolecular interactions between the HESs and BPA. A negative value of H^E indicates an exothermic mixing process, while a positive value shows an endothermic process. In ideal solutions, H^E is zero, whereas in non-ideal solutions, mixing leads to non-zero H^E values. As it is illustrated in Fig. 1, the H^E values across all compositions in Ment-based HESs are more negative than those in Thym-based solvents, suggesting more favorable interactions between the Ment-based solvents and BPA. For the HESs, including Thym: OctOl, Thym: DecOl, and Thym: Ment, the transition from positive to negative values of ln γ^{∞} led to more significant changes in H^E values. The resulting data underscores the importance of composition in determining the strength of the intermolecular interactions between the analyte and the HESs.

Based on the COSMO-RS predicted results, seven HESs with ln γ^{∞} values below −1.0 were selected and experimentally prepared as promising solvents for the extraction of BPA. The extraction efficiency of the HESs was evaluated by calculating the ER % given by Eq. (1).

$$ER\% = \frac{C_f V_f}{C_0 V_{aq}} \times 100 \quad (1)$$

Where C_f and C_0 are BPA concentrations in the separated HES-rich phase and sample solution, respectively, and V_f and V_{aq} are volumes of the extract and the aqueous phase, respectively. To achieve this, 100 μL of each HES was injected into the 10 mL sample solution, containing 100 μg/L of BPA, and the solution was vortexed for 5 min to facilitate the transfer of BPA into the HES. Following this, the mixture was centrifuged at 2795 g for 4 min to separate the HES-rich phase. The extract was subsequently collected on the top surface of the sample tube after solidification and transferred to a clean vial before HPLC analysis.

Among the tested HESs, Thym: OctOl (1:2), Ment: OctOl (2:1), Ment: DecOl (2:1), and Ment: OctA (2:1) resulted in the extraction efficiencies ranging from 65 % to 70 % and were selected as promising solvents to extract BPA (Fig. S1). The density of these systems was experimentally measured, while viscosity values were only obtained from COSMO-RS predictions as summarized in Table 2. The higher ER % of Ment: OctA is attributed to its lower viscosity, as predicted by COSMO-RS , which facilitates the mass transfer of BPA from the aqueous phase to the HES. Additionally, the lower viscosity of Ment: OctA enhances the phase separation after the extraction process. A more viscous solvent may not

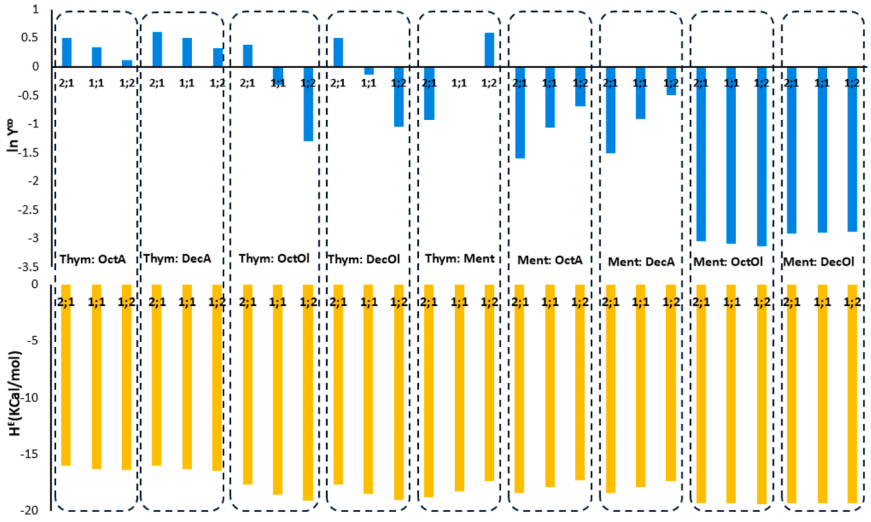

Fig. 1. COSMO-RS predicted ln γ^{∞} and H^E values for BPA in different Thym and Ment-based HESs at 298.15 K.

Table 2
COSMO-RS predicted densities and viscosities of the parent components and four selected HESs.

Component/HES	Density (g/mL)		Viscosity (cP)
	Pred.	Exp.	Pred.
Thym	0.9562	0.9610	6.13
Ment	0.8838	0.8932	11.14
OctA	0.9169	0.9070	17.98
OctOl	0.8191	0.8271	12.26
DecOl	0.8257	0.8360	21.45
Thym: OctOl (1:2)	0.8743	0.9220	7555.08
Ment: OctOl (2:1)	0.8771	0.8840	37,797.81
Ment: DecOl (2:1)	0.8721	0.8660	78,046.14
Ment: OctA (2:1)	0.8912	0.9150	4485.21

be separated easily from the sample solution, making it difficult to collect on the top surface.

In this study, the extraction efficiency of the liquid components, including OctA, OctOl, and DecOl was also investigated at room temperature. The LLME procedure was conducted under the same extraction conditions as described in the previous step for the HESs, and the ER % of the components was compared to the HESs formed by combining Ment and Thym with these precursors. The extraction efficiencies of OctA, OctOl, and DecOl were 53 %, 46 %, and 18 %, respectively, which were found to be lower than those of the four potential HESs selected in the previous step. This comparative analysis aims to explain the contribution of each component to the overall extraction efficiency, highlighting the synergistic effects of HBAs and HBDs, which enhance the interactions of the HESs with BPA. In contrast, pure components lack such cooperative hydrogen bonding, which limits mass transfer and results in lower extraction efficiency.

To further understand the interactions of BPA with the selected HESs,

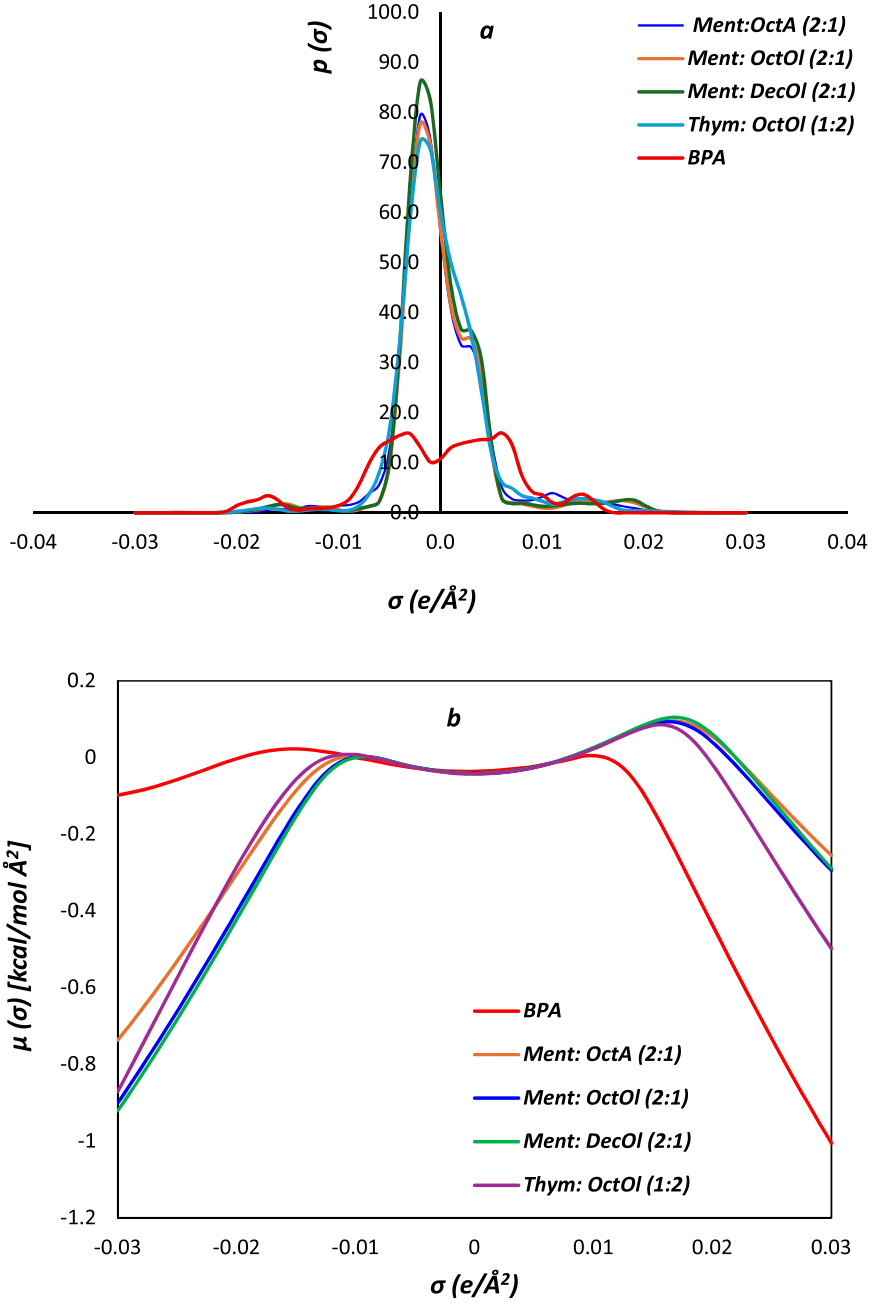

Fig. 2. Predicted σ-profiles (a) and σ-potentials (b) of Thym: OctOl (1:2), Ment: OctOl (2:1), Ment: DecOl (2:1), Ment: OctA (2:1), and BPA by COSMO-RS.

the sigma profiles (σ-profile) and sigma potentials (σ-potential) of BPA and HESs were obtained using COSMO-RS, as illustrated in Fig. 2. According to Fig. 2a, BPA exhibits peaks in both the HBA and HBD regions. The σ-profile peaks for all HESs are predominantly located in a non-polar region, confirming their hydrophobic characteristics. Additionally, all the HESs display peaks in both HBA and HBD regions, indicating their ability to interact with both polar and non-polar analytes. The σ-potential of BPA (Fig. 2b) shows a significant affinity for HBDs, suggesting that solvents with hydrogen-bond donating capabilities are likely to promote more favorable HB interactions with BPA. All four HESs display HBA and HBD segments in their σ-potentials with similar intensities, while Ment: OctA exhibits a higher extraction efficiency, which can be attributed to its lower viscosity and enhanced mass transfer of the analyte.

We also conducted quantum chemistry calculations to investigate the properties of the selected HESs and their interactions with BPA. The geometries of Ment: OctOl (2:1), Ment: DecOl (2:1), Ment: OctA (2:1), and Thym: OctOl (1:2) were obtained using Gaussian09 at the B3LYP/6–31+*G*(d,p) level of theory [22]. Typical structures of the mentioned HESs are shown in Fig. 3. As illustrated, HB interactions are present between the components of all HESs (indicated by dashed lines). The interaction energy (ΔE) for HESs was then calculated using the difference between the energy of each HES and the energies of the parent components as:

$$\Delta E = E_{HES} - \sum E_{component} \quad (2)$$

The absolute values of interaction energy (|ΔE|) of the HESs in kcal/mol are as follows: Ment: DecOl (0.81) < Ment: OctOl (3.04) < Thym: OctOl (4.73) < Ment: OctA (9.17). Thus, the strength of HB interactions in Ment: OctA is larger than that of other HESs. This QM study aims to evaluate the ability of these HESs to extract BPA and to find a relationship between QM descriptors and extraction efficiency.

Typical structures of the HES: BPA complexes are shown in Fig. 4. Each HES: BPA complex exhibits three HB interactions. The sum of hydrogen bond lengths ($\sum d_{HB}$) for the HES: BPA complexes was estimated to be 4.797 Å, 4.764 Å, 4.549 Å, and 4.180 Å for Ment: DecOl, Ment: OctOl, Thym: OctOl, and Ment: OctA, respectively. This suggests that the HB lengths in the Ment: OctA: BPA complex are shorter than in the other complexes, confirming its higher extraction efficiency. The acidic moiety in Ment: OctA contributes dual HBA and HBD characteristics, enabling stronger and more directional interactions with BPA, which is less pronounced in other systems. In contrast, the aromatic and more rigid structure of Thym restricts conformational flexibility and limits optimal HB alignment with BPA, resulting in weaker overall interactions for the Thym: OctOl system.

Additionally, energies of the highest occupied molecular orbital (HOMO), lowest unoccupied molecular orbital (LUMO), energy gap (E_{gap}), and softness (s) of the HES: BPA complexes were assessed (Table 3) to uncover QM descriptors related to the extraction efficiency values. Also, hardness (H) and softness (S) were obtained using the following equations:

$$Hardness = (E_{LUMO} - -E_{HOMO})/2 \quad (3)$$

$$Softness = 1/Hardness \quad (4)$$

Results revealed a linear relationship between E_{gap} and ER % values, with a linear regression coefficient of R^2=0.95. A decrease in E_{gap} values corresponds to an increase in the ER %, indicating that higher ER % values contribute to the formation of the HES: BPA complexes with greater softness. Accordingly, atomic charges of HESs were calculated to investigate a relationship between these descriptors and E_{gap} values. The order of sum of atomic charges on oxygen atoms of HESs (ΣQ_O) in e was: Ment: OctA (−2.243) < Thym: OctOl (−1.890) < Ment: OctOl (−1.659) < Ment:DecOl (−1.629). Thus, Ment: OctA, with the lowest E_{gap} value and the greatest softness, has the most negative ΣQ_O value among the

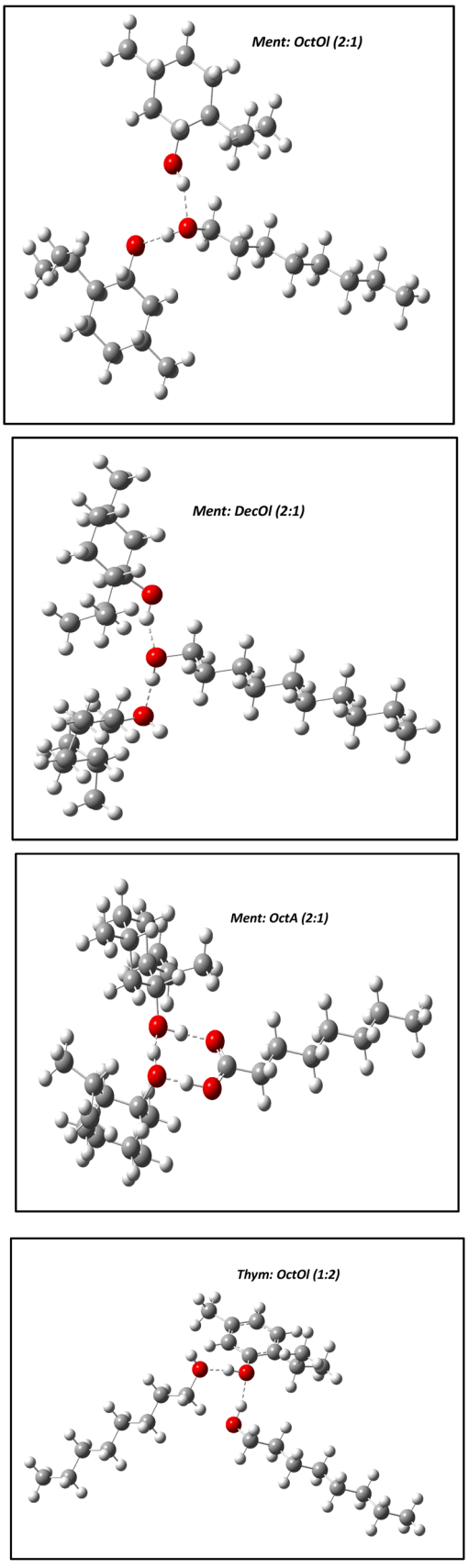

Fig.3. Representative structures of the selected HESs generated by QM calculations. Dashed lines indicate HB interactions.

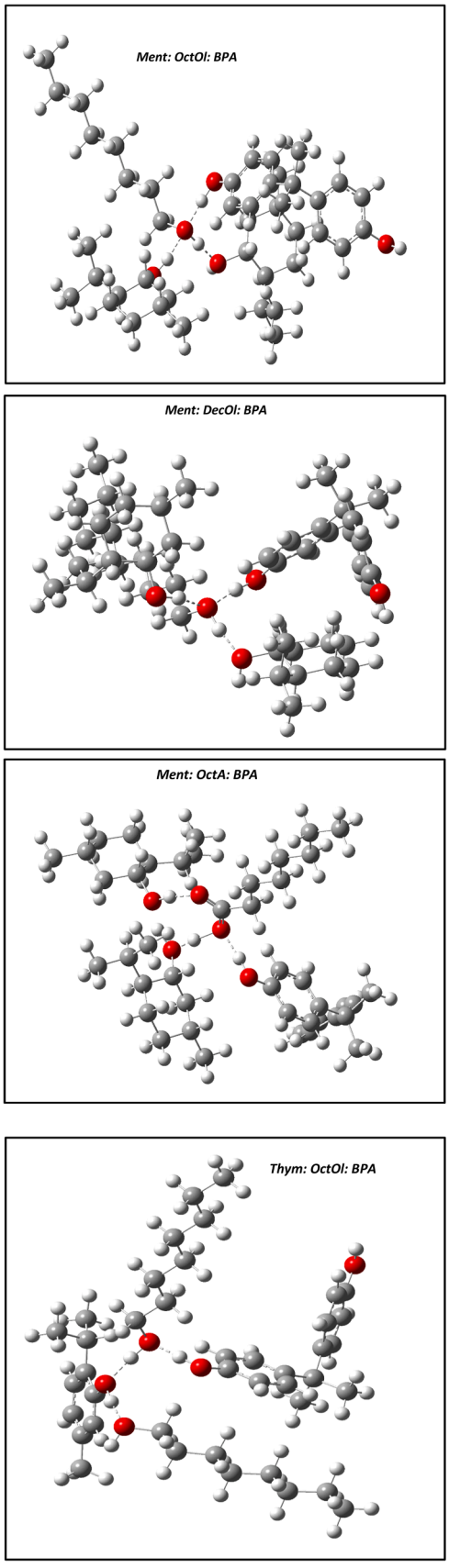

Fig. 4. HB interactions between the selected HESs and BPA.

Table 3
Energies of HOMO and LUMO, energy gap, hardness, and softness values of the HES: BPA complexes, presented in eV.

ES: BPA	E_{HOMO}	E_{LUMO}	E_{gap}	H	S
Ment: OctOl: BPA	−5.392	−0.041	5.352	−2.676	−0.374
Ment: DecOl: BPA	−5.448	−0.045	5.403	−2.702	−0.370
Ment: OctA: BPA	−5.342	−0.154	5.187	−2.594	−0.386
Thym: OctOl: BPA	−5.256	0.139	5.395	−2.698	−0.371

studied HESs. As noted above, this HES has the highest ER % value. Overall, the distribution of atomic charges on the oxygen atoms of the HESs influences the E_{gap} and softness values at the molecular level, which is reflected experimentally in the ER % values.

The distributions of electron charge density on HOMOs and LUMOs were also analyzed for all HES: BPA complexes. The red and green colours represent negative and positive moieties, respectively. Frontier molecular orbital (FMO) diagrams of the HES: BPA complexes are displayed in Fig. 5. Results showed that the HOMO is primarily distributed on BPA in all HES: BPA complexes, but fully covers BPA in the Ment: OctA: BPA complex. Conversely, the LUMO is located on Ment, Ment-BPA, acidic part of OctA, and Thym in the Ment: OctOl: BPA, Ment: DecOl: BPA, Ment: OctA: BPA, and Thym: OctOl: BPA complexes, respectively. The Ment: OctA: BPA complex has the lowest E_{LUMO} value among the other complexes. The distribution of LUMO on the acidic part of OctA, which exhibits the dual HBA and HBD characteristics, contributes to the stability of this molecular orbital and decreases its energy gap. Therefore, OctA component plays a crucial role in enhancing the extraction efficiency of Ment: OctA as an HES and reducing the E_{gap} of the Ment: OctA: BPA complex.

Furthermore, CD curves of the HES: BPA complexes were generated by comparing charge densities under normal conditions and in the presence of an electric field. The minimum points in Fig. S2 indicate the number of electrons in the left part of the complexes due to the electric field. Results showed that the number of electrons on the left side of the Ment: OctOl: BPA and Ment: OctA: BPA is 1.3, which is larger than in other complexes, aligning with the extraction efficiency of these HESs.

Our research group has recently explored the innovative concept of switchable solvents, which enables HESs to change their nature from hydrophobic to hydrophilic [16–18,24]. To achieve this, changing pH triggered the reversible phase conversion. For the switchable pH-LLME process, 95 μL of Ment: OctA (2:1) was added to 10 mL of an aqueous sample solution containing 100 μg/L of BPA standard, followed by the addition of 100 μL KOH (4.5 M) to create a single phase with water. The sample tube was then shaken for 1 min to facilitate the mass transfer of BPA into the extract. The addition of 100 μL of HCl (5.0 M) reversed the phase hydrophobicity of the HES, resulting in the formation of two distinct phases with the aqueous solution. Finally, the extract was collected from the top surface of the sample tube after the solidification process. The HES composed of Ment: OctA (2:1) resulted in higher extraction efficiency (75 %) compared to other HESs, making it a promising candidate for the subsequent LLME of BPA. Increasing pH deprotonates OctA in the Ment: OctA system due to the formation of the octanoate anion. Upon adding HCl, the octanoate anions protonate back to OctA. This reversible phase transition occurred under mild conditions and does not involve hydrolysis and esterification of the HES components, thereby preserving the chemical integrity of the system. The switchability of the Ment: OctA system through the addition of base and acid provides a versatile approach to extract BPA from different samples, including water and plastic-packed dairy products. The adaptability improves the sustainability of the proposed method by minimizing waste generation. Moreover, the Ment: OctA system exhibits low water solubility, efficient and stable switching behavior achieved through simple pH adjustment, along with good physicochemical stability. Compared with other switchable solvents containing synthetic amines, this system offers tunable viscosity and polarity via the selection of

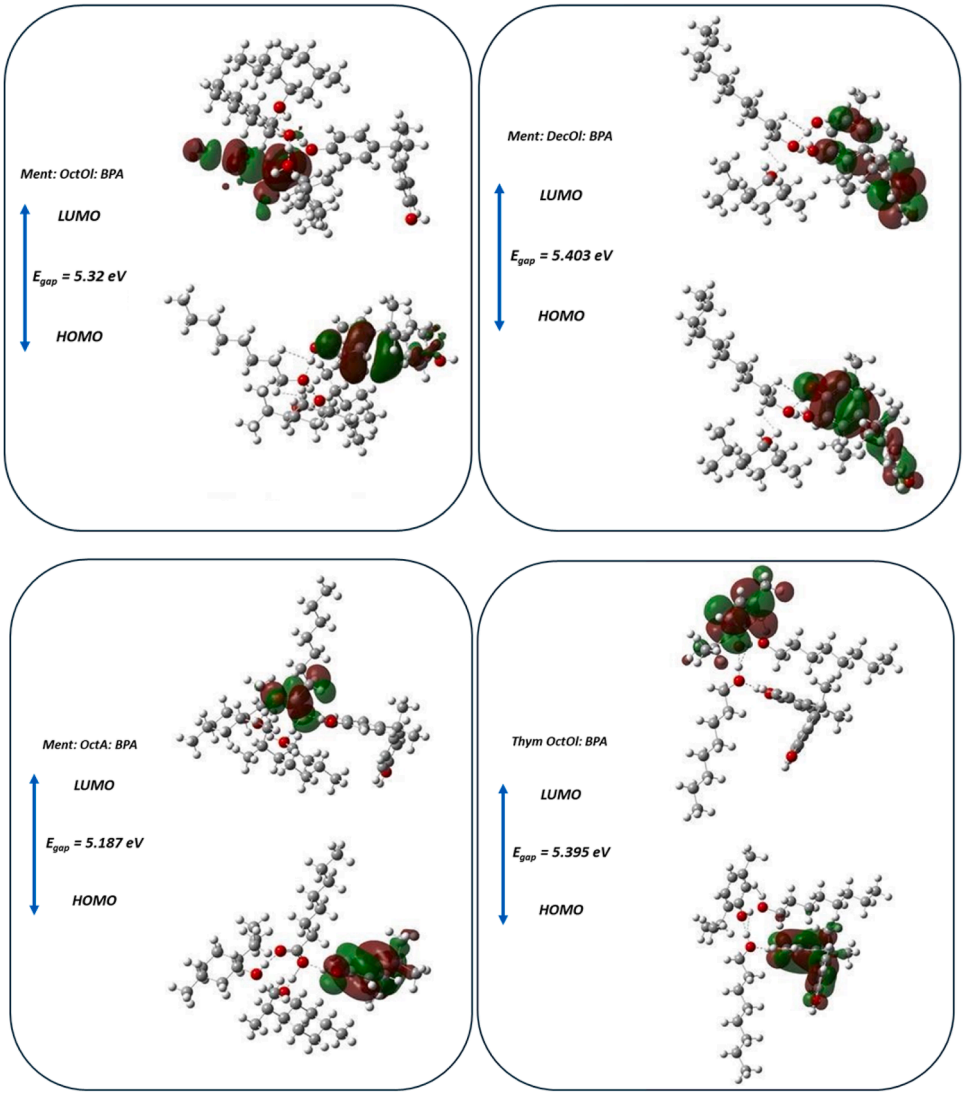

Fig. 5. Distributions of HOMO and LUMO on the HES: BPA complexes.

carboxylic acids. Additionally, reduced solvent loss improves its suitability for the extraction of BPA from complex matrices.

4. Optimization of the extraction conditions

CCD was implemented to determine the optimal extraction conditions of the LLME process due to its flexibility and robustness. During the trials, the data were modelled using Eq. (5), resulting in a correlation coefficient ($R^2 = 0.9419$), as shown in Table S2.

$$\%ER = 51.00 - 5.7X_1 + 6.87X_2 - 18.89X_3 - 1.25X_1X_2 - 1.04X_1X_3 + 16.25X_2X_3 - 8.02X_1^2 - 12.01X_2^2 - 2.02X_3^2 \quad (5)$$

Accordingly, the significant terms identified in the quadratic model include single factors (volume of HES (X_1), concentration of KOH (X_2), and volume of HCl (X_3)), the two-factor interaction X_2X_3, and the single-factor self-interactions X_2^2 and X_3^2. This indicates that the combined effects of factors X_2 and X_3 were not simply additive, as the effect of one factor depends on the level of the other. Specifically, the concentration of KOH and the volume of HCl may exhibit synergistic effects and/or non-linear responses. The combined influence on the extraction yield could therefore be greater or less than the sum of their individual effects. Such interactions suggest a complex relationship between these variables, where one enhances or modifies the effect of the other. Similar conclusions were drawn in this study, as both individual factors and their interactions significantly impacted the extraction process.

Fig. S3 presents three-dimensional (3D) plots of the predicted responses, visually illustrating the nonlinear interactions among the variables. The analysis of these plots revealed consistent trends throughout the model, characterized by smoothly convex response surfaces. After selecting the most appropriate model, the optimal conditions were determined by evaluating the combined effects of the variables and their interactions on the response. The optimized conditions were 95 µL of HES, 100 µL of 4.5 M KOH, and 100 µL of 5.0 M HCl. Under these conditions, the predicted ER % for BPA was 74.5 %, while the experimentally obtained ER % was 75 %. To ensure complete reporotonation and phase conversion, the number of millimoles of HCl must be equal to or greater than that of KOH. Therefore, this stoichiometric requirement was incorporated into the CCD to ensure complete and reversible phase conversion, while maximizing the extraction efficiency.

5. Validation of the microextraction method

The analytical performance of the developed pH-switchable LLME method was investigated under the optimized conditions. To obtain the calibration curve, seven concentrations of BPA were subjected to the

optimized LLME process, demonstrating that acceptable linearity was observed in the range of 0.15–200 μg/L with R^2 value of 0.9975. The limit of detection (LOD) and limit of quantification (LOQ) were found to be 0.05 μg/L and 0.15 μg/L, based on the signal-to-noise ratio of 3 and 10, respectively. The enrichment factor, calculated by comparing the concentration of BPA before and after the extraction process, was found to be 180. The intra- and inter-day repeatability were investigated at a concentration level of 100 μg/L ($n = 5$), reported as relative standard deviation (RSD %). Accordingly, the intra- and inter-day RSD % were 2.8 % and 5.3 %, respectively.

LLME is one of the most widely used extraction techniques to extract BPA from diverse matrices due to its simplicity and ease of operation. Recently, different types of ESs have been used for BPA in the LLME process. The analytical features of our developed method are comparable with those of previously published studies (Table 4). A significant advantage of our method is that it does not require a dispersive solvent, which is usually used to facilitate the extraction process. Additionally, the reversible phase separation eliminates the need for unnecessary centrifugation and reduces extraction time. Application of COSMO-RS and quantum chemistry allows for the screening of the most effective solvent for BPA extraction, minimizing the time and resources required for experimental screening. Furthermore, computational methods help in understanding the underlying intermolecular interactions between the solute and solvents.

6. Evaluation of the method's environmental impact

The environmental impact of the entire analytical approach and the sample preparation method was evaluated using greenness assessment tools, including AGREE and AGREEprep, based on different principles of green chemistry. The results are illustrated with color codes, where green indicates the maximum score (1.0) and red the minimum (0.0). The lowest scores were observed for principle 3 in AGREE (Fig. 6a) and principle 1 in AGREEprep (Fig. 6b), which can be attributed to the off-line analysis procedure. The use of portable devices could improve this limitation by allowing *in situ* measurements.

Additionally, the practicality of the developed pH-switchable LLME procedure was evaluated by the blue applicability grade index (BAGI).

Table 4
Comparison of liquid phase extraction techniques for the determination of BPA in various samples.

Extraction technique	Solvent	LOD (μg/L)	LOQ (μg/L)	Intra-day RSD %	Real sample	Ref.
VA-LLME	TAC: DecA	0.06	0.3	4.65	Food-canned plastics	[12]
LLE	Ment: Formic acid and Ment: propionic acid	12	39.9	-	Water samples	[9]
LLME	Thym: DodecA	0.02	-	2.20	Water samples	[20]
DLLME	Sodium octanoate	0.03	0.12	0.80	Water and beverage samples	[25]
DLLME	Ment: AcetA	50	166	-	Sludge samples	[19]
VA-BS-DLLME	OctOl: hexane	0.08	0.26	2.85	Water samples	[26]
LLME	Ment: OctA	0.05	0.15	2.80	Water and dairy products	This work

DLLME: Dispersive liquid-liquid microextraction; DodecA: Dodecanoic acid; VA-LLME: Vortex-assisted liquid-liquid microextraction; VA-BS-DLLME: Vortex-assisted binary solvent dispersive liquid–liquid microextraction; TAC: Trioctylmethyl ammonium chloride.

Fig. 6. Evaluation of the sustainability and applicability of the developed pH-switchable LLME using (a) AGREE, (b) AGREEprep, and (b) BAGI.

This tool evaluates ten different criteria and generates an asteroid-shaped pictogram, where dark blue corresponds to the highest score, and white indicates no compliance with the criteria set. For an analytical method to be considered practical, a score above 60 is required. Our method achieved a score of 65 (Fig. 6c), confirming its applicability.

7. Application of the pH-switchable LLME to dairy products and water samples analysis

The optimized pH-switchable LLME was applied to extract BPA from water samples and plastic-packed dairy products, such as milk, cocoa milk, and coffee milk, with the results summarized in Table 5. BPA is a commonly used monomer in the plastic industry. As it is not covalently bound to the polymer matrix, BPA can migrate from plastic over time. Its migration is accelerated by factors such as elevated temperature, ageing of the plastic materials, and contact with acids and bases. Water contamination by BPA can occur through different pathways, including wastewater treatment, industrial effluents, and plastic degradation. The use of coated pipes and epoxy resins can further increase BPA concentration in water, particularly with hot water systems. Prolonged contact with plastic-packed samples also promotes BPA migration into the sample. Accordingly, the sampling protocol was designed to include both plastic and metal water tanks under different environmental conditions to capture the effect of thermal and photochemical stress on the BPA leaching process.

All water samples stored in plastic tanks exposed to sunlight exhibited detectable levels of BPA, whereas only some tanks situated in shade contained BPA. Moreover, BPA concentrations in plastic tanks exposed to the sunlight were higher than those in shadow-located tanks, confirming that elevated temperature enhances molecular mobility and the leaching of BPA molecules into the water samples. Notably, BPA was not detected in metallic tanks during both seasons, underscoring the effect of storage materials on the released concentration of the analyte.

Regarding the dairy products, BPA was not detected in any samples analyzed; most likely, they were stored at low temperatures. It can also be attributed to the short shelf lives of these single-use plastics designed for dairy products, reducing the opportunity for leaching. In addition, the complex composition of dairy products presents inherent analytical challenges, as BPA can associate with milk proteins through non-covalent interactions and partition into the lipid phase, thereby decreasing the freely extractable fraction of the analyte. Such lipid interferences and protein bonding can hinder BPA release and complicate the extraction process compared to the simple aqueous samples.

Finally, to assess the method's reliability, the determination of BPA in spiked water and dairy products was carried out (Table S3), yielding the relative recoveries between 95 % and 109 %, demonstrating both accuracy and precision.

8. Conclusion

In this study, COSMO-RS was used to screen the Thym and Ment-based HESs for the extraction of BPA from water samples and dairy products. Of the twenty-seven hydrophobic HESs designed and

Table 5
Analysis of water samples using the pH-switchable LLME method.

Sample No.	Sampling season	Sampling location	Tank type	Tank location	Concentration (Mean ± SD, μg/L)
1	Summer	Garden House	Plastic	Exposed to the sun	10.6 ± 0.4
2	Summer	Garden House	Plastic	Exposed to the sun	22.3 ± 1.3
3	Summer	Garden House	Plastic	Exposed to the sun	11.7 ± 0.6
4	Summer	Garden House	Plastic	Exposed to the sun	35.4 ± 2.3
5	Summer	Garden House	Plastic	Exposed to the sun	67.2 ± 3.5
6	Summer	Garden House	Plastic	In the shadow	10.3 ± 0.5
7	Summer	Garden House	Plastic	In the shadow	5.2 ± 0.3
8	Summer	Garden House	Plastic	In the shadow	n.d.
9	Summer	Garden House	Plastic	In the shadow	8.6 ± 0.5
10	Summer	Garden House	Plastic	In the shadow	n.d.
11	Summer	Garden House	Metal	Exposed to the sun	n.d.
12	Summer	Garden House	Metal	Exposed to the sun	n.d.
13	Summer	Garden House	Metal	Exposed to the sun	n.d.
14	Summer	Garden House	Metal	Exposed to the sun	n.d.
15	Summer	Garden House	Metal	Exposed to the sun	n.d.
16	Summer	Garden House	Metal	In the shadow	n.d.
17	Summer	Garden House	Metal	In the shadow	n.d.
18	Summer	Garden House	Metal	In the shadow	n.d.
19	Summer	Garden House	Metal	In the shadow	n.d.
20	Summer	Garden House	Metal	In the shadow	n.d.
21	Summer	Villa House	Plastic	Exposed to the sun	31.9 ± 1.8
22	Summer	Villa House	Plastic	Exposed to the sun	20.3 ± 1.2
23	Summer	Villa House	Plastic	Exposed to the sun	51.5 ± 3.4
24	Summer	Villa House	Plastic	Exposed to the sun	17.6 ± 0.9
25	Summer	Villa House	Plastic	Exposed to the sun	28.8 ± 2.2
26	Summer	Villa House	Plastic	In the shadow	n.d.
27	Summer	Villa House	Plastic	In the shadow	8.5 ± 0.5
28	Summer	Villa House	Plastic	In the shadow	n.d.
29	Summer	Villa House	Plastic	In the shadow	3.7 ± 0.3
30	Summer	Villa House	Plastic	In the shadow	10.1 ± 0.7
31	Summer	Villa House	Metal	Exposed to the sun	n.d.
32	Summer	Villa House	Metal	Exposed to the sun	n.d.
33	Summer	Villa House	Metal	Exposed to the sun	n.d.
34	Summer	Villa House	Metal	Exposed to the sun	n.d.
35	Summer	Villa House	Metal	Exposed to the sun	n.d.
36	Summer	Villa House	Metal	In the shadow	n.d.
37	Summer	Villa House	Metal	In the shadow	n.d.
38	Summer	Villa House	Metal	In the shadow	n.d.
39	Summer	Villa House	Metal	In the shadow	n.d.
40	Summer	Villa House	Metal	In the shadow	n.d.
41	Summer	Apartment	Plastic	Exposed to the sun	18.7 ± 1.3
42	Summer	Apartment	Plastic	Exposed to the sun	n.d.
43	Summer	Apartment	Plastic	Exposed to the sun	29.1 ± 1.9
44	Summer	Apartment	Plastic	Exposed to the sun	16.3 ± 0.8
45	Summer	Apartment	Plastic	Exposed to the sun	n.d.
46	Summer	Apartment	Plastic	In the shadow	n.d.
47	Summer	Apartment	Plastic	In the shadow	11.5 ± 0.6
48	Summer	Apartment	Plastic	In the shadow	3.4 ± 0.2
49	Summer	Apartment	Plastic	In the shadow	n.d.
50	Summer	Apartment	Plastic	In the shadow	4.6 ± 0.3
51	Summer	Apartment	Metal	Exposed to the sun	n.d.
52	Summer	Apartment	Metal	Exposed to the sun	n.d.
53	Summer	Apartment	Metal	Exposed to the sun	n.d.
54	Summer	Apartment	Metal	Exposed to the sun	n.d.
55	Summer	Apartment	Metal	Exposed to the sun	n.d.
56	Summer	Apartment	Metal	In the shadow	n.d.
57	Summer	Apartment	Metal	In the shadow	n.d.

(continued on next page)

Table 5 (*continued*)

Sample No.	Sampling season	Sampling location	Tank type	Tank location	Concentration (Mean ± SD, µg/L)
58	Summer	Apartment	Metal	In the shadow	n.d.
59	Summer	Apartment	Metal	In the shadow	n.d.
60	Summer	Apartment	Metal	In the shadow	n.d.
61	Winter	Garden House	Plastic	Exposed to the sun	13.2 ± 0.6
62	Winter	Garden House	Plastic	Exposed to the sun	15.4 ± 1.1
63	Winter	Garden House	Plastic	Exposed to the sun	n.d.
64	Winter	Garden House	Plastic	Exposed to the sun	8.1 ± 0.5
65	Winter	Garden House	Plastic	Exposed to the sun	4.7 ± 0.3
66	Winter	Garden House	Plastic	In the shadow	n.d.
67	Winter	Garden House	Plastic	In the shadow	2.9 ± 0.2
68	Winter	Garden House	Plastic	In the shadow	n.d.
69	Winter	Garden House	Plastic	In the shadow	3.8 ± 0.3
70	Winter	Garden House	Plastic	In the shadow	n.d.
71	Winter	Garden House	Metal	Exposed to the sun	n.d.
72	Winter	Garden House	Metal	Exposed to the sun	n.d.
73	Winter	Garden House	Metal	Exposed to the sun	n.d.
74	Winter	Garden House	Metal	Exposed to the sun	n.d.
75	Winter	Garden House	Metal	Exposed to the sun	n.d.
76	Winter	Garden House	Metal	In the shadow	n.d.
77	Winter	Garden House	Metal	In the shadow	n.d.
78	Winter	Garden House	Metal	In the shadow	n.d.
79	Winter	Garden House	Metal	In the shadow	n.d.
80	Winter	Garden House	Metal	In the shadow	n.d.
81	Winter	Villa House	Plastic	Exposed to the sun	5.5 ± 0.4
82	Winter	Villa House	Plastic	Exposed to the sun	1.8 ± 0.1
83	Winter	Villa House	Plastic	Exposed to the sun	n.d.
84	Winter	Villa House	Plastic	Exposed to the sun	6.2 ± 0.3
85	Winter	Villa House	Plastic	Exposed to the sun	1.5 ± 0.1
86	Winter	Villa House	Plastic	In the shadow	n.d.
87	Winter	Villa House	Plastic	In the shadow	2.1 ± 0.1
88	Winter	Villa House	Plastic	In the shadow	n.d.
89	Winter	Villa House	Plastic	In the shadow	n.d.
90	Winter	Villa House	Plastic	In the shadow	0.8 ± 0.1
91	Winter	Villa House	Metal	Exposed to the sun	n.d.
92	Winter	Villa House	Metal	Exposed to the sun	n.d.
93	Winter	Villa House	Metal	Exposed to the sun	n.d.
94	Winter	Villa House	Metal	Exposed to the sun	n.d.
95	Winter	Villa House	Metal	Exposed to the sun	n.d.
96	Winter	Villa House	Metal	In the shadow	n.d.
97	Winter	Villa House	Metal	In the shadow	n.d.
98	Winter	Villa House	Metal	In the shadow	n.d.
99	Winter	Villa House	Metal	In the shadow	n.d.
100	Winter	Villa House	Metal	In the shadow	n.d.
101	Winter	Apartment	Plastic	Exposed to the sun	13.5 ± 0.8
102	Winter	Apartment	Plastic	Exposed to the sun	11.2 ± 1.0
103	Winter	Apartment	Plastic	Exposed to the sun	7.4 ± 0.5
104	Winter	Apartment	Plastic	Exposed to the sun	n.d.
105	Winter	Apartment	Plastic	Exposed to the sun	5.1 ± 0.2
106	Winter	Apartment	Plastic	In the shadow	n.d.
107	Winter	Apartment	Plastic	In the shadow	1.9 ± 0.1
108	Winter	Apartment	Plastic	In the shadow	n.d.
109	Winter	Apartment	Plastic	In the shadow	0.7 ± 0.1
110	Winter	Apartment	Plastic	In the shadow	n.d.
111	Winter	Apartment	Metal	Exposed to the sun	n.d.
112	Winter	Apartment	Metal	Exposed to the sun	n.d.
113	Winter	Apartment	Metal	Exposed to the sun	n.d.
114	Winter	Apartment	Metal	Exposed to the sun	n.d.
115	Winter	Apartment	Metal	Exposed to the sun	n.d.

(*continued on next page*)

Table 5 (*continued*)

Sample No.	Sampling season	Sampling location	Tank type	Tank location	Concentration (Mean ± SD, µg/L)
116	Winter	Apartment	Metal	In the shadow	n.d.
117	Winter	Apartment	Metal	In the shadow	n.d.
118	Winter	Apartment	Metal	In the shadow	n.d.
119	Winter	Apartment	Metal	In the shadow	n.d.
120	Winter	Apartment	Metal	In the shadow	n.d.

SD: Standard deviation ($n = 3$).
n.d.: Not detected.

screened, seven were experimentally prepared to validate the computational predictions. The experimental results revealed that Thym: OctOl (1:2), Ment: OctOl (2:1), Ment: DecOl (2:1), and Ment: OctA (2:1) were among the best solvents and compositions. The hydrophobicity of these HESs was then switched by changing the pH, with Ment: OctA (2:1) yielding the highest extraction efficiency. Previous studies employing COSMO-RS have primarily focused on the screening of HESs for the extraction of BPA mainly from simple aqueous samples, where the solvent-solute interactions can be reasonably approximated under ideal conditions. In contrast, this study addresses the extraction of BPA from more complex matrices, containing macromolecules, such as proteins and lipids, that can interact competitively with the PBA and the extraction solvent, affecting the phase behavior, mass transfer, and introducing matrix interferences that are not accounted for in COSMO-RS predictions. Therefore, while COSMO-RS is a powerful tool for the initial solvent selection, it cannot fully describe mass transfer limitations and matrix-induced effects in real food samples. Our work complements the previous theoretical studies by experiments, demonstrating the performance and selectivity of HESs in complex matrices.

Additionally, the efficiency of HB interactions between the parent components of the HESs and HES-BPA complexes was investigated using quantum chemistry calculations. Accordingly, the most stable HB was observed in the Ment: OctA (2:1) system, enhancing its affinity with the target analyte. Finally, the developed pH-switchable LLME process was evaluated using AGREE, AGREEprep, and BAGI, achieving scores of 0.61, 0.66, and 65, respectively, which support the sustainability and applicability of the developed microextraction approach.

CRediT authorship contribution statement

Nazir Fattahi: Validation, Methodology, Formal analysis. **Parvin Zohrabi:** Validation, Methodology, Conceptualization. **Pouya Karimi:** Writing – original draft, Software. **Filipe Hobi Bordón Sosa:** Writing – review & editing, Software. **Beshare Hashemi:** Writing – review & editing, Writing – original draft, Validation, Supervision, Methodology, Investigation, Conceptualization. **Fereshteh Shiri:** Writing – original draft, Validation, Software.

Declaration of competing interest

The authors declare that they have no known competing financial interests or personal relationships that could have appeared to influence the work reported in this paper.

Acknowledgment

Research reported in this publication was supported by the Elite Researcher Grant Committee (under award number: 4021421) from the National Institute for Medical Research Development (NIMAD), Tehran, Iran. Also, the authors gratefully acknowledge the Research Council of Kermanshah University of Medical Sciences for the financial support (Grant Number: 4040334). This work was also partly developed within the scope of the project CICECO-Aveiro Institute of Materials, UIDB/50011/2020 (DOI 10.54499/UIDB/50011/2020), UIDP/50011/2020 (DOI 10.54499/ UIDP/50011/2020) & LA/P/0006/2020 (DOI 10.54499/LA/P/0006/ 2020), financed by national funds through the FCT/MCTES (PIDDAC). Filipe H. B. Sosa acknowledges FCT for the research contract CEECIND/07209/2022 (DOI 10.54499/2022.07209.CEECIND/CP1720/CT0019) under the Scientific Stimulus – Individual Call.

Supplementary materials

Supplementary material associated with this article can be found, in the online version, at doi:10.1016/j.chroma.2026.466709.

Data availability

Data will be made available on request.

References

[1] M.-K. Kim, K.-D. Zoh, Occurrence and removals of micropollutants in water environment, Environ. Eng. Res. 21 (4) (2016) 319–332, https://doi.org/10.4491/eer.2016.115.
[2] C. Nicolucci, S. Rossi, C. Menale, E.M. Del Giudice, L. Perrone, P. Gallo, D.G. Mita, N. Diano, A high selective and sensitive liquid chromatography–tandem mass spectrometry method for quantization of BPA urinary levels in children, Anal. Bioanal. Chem. 405 (2013) 9139–9148, https://doi.org/10.1007/s00216-013-7342-y.
[3] Y. Ma, H. Liu, J. Wu, L. Yuan, Y. Wang, X. Du, R. Wang, P.W. Marwa, P. Petlulu, X. Chen, The adverse health effects of bisphenol A and related toxicity mechanisms, Environ. Res. 176 (2019) 108575, https://doi.org/10.1016/j.envres.2019.108575.
[4] J. Torres-García, M. Ahuactzin-Pérez, F. Fernández, D.V. Cortés-Espinosa, Bisphenol A in the environment and recent advances in biodegradation by fungi, Chemosphere 303 (2022) 134940, https://doi.org/10.1016/j.chemosphere.2022.134940.
[5] A. Shankar, S. Teppala, C. Sabanayagam, Urinary bisphenol a levels and measures of obesity: results from the national health and nutrition examination survey 2003–2008, Int. Sch. Res. Notices. 2012 (1) (2012) 965243, https://doi.org/10.5402/2012/965243.
[6] C. Polesca, H. Passos, A.C. Sousa, N.M. Tue, J.A. Coutinho, T. Kunisue, M.G. Freire, Sustainable pretreatment of blood samples using hydrophobic eutectic solvents to improve the detection of bisphenol A, Green Chem. 27 (1) (2025) 200–208, https://doi.org/10.1039/D4GC03396E.
[7] C. Florindo, N.V. Monteiro, B.D. Ribeiro, L. Branco, I. Marrucho, Hydrophobic deep eutectic solvents for purification of water contaminated with bisphenol-A, J. Mol. Liq. 297 (2020) 111841, https://doi.org/10.1016/j.molliq.2019.111841.
[8] D. Rodríguez-Llorente, P. Navarro, R. Santiago, V.I. Águeda, S. Álvarez-Torrellas, J. García, M. Larriba, Extractive removal and recovery of bisphenol A from aqueous solutions using terpenoids and hydrophobic eutectic solvents, J. Environ. Chem. Eng. 9 (5) (2021) 106128, https://doi.org/10.1016/j.jece.2021.106128.
[9] Y. An, K.H. Row, Evaluation of menthol-based hydrophobic deep eutectic solvents for the extraction of bisphenol A from environment water, Anal. Lett. 54 (9) (2021) 1533–1545, https://doi.org/10.1080/00032719.2020.1811716.
[10] A.S. Alnaimat, M.C. Barciela-Alonso, P. Bermejo-Barrera, Determination of bisphenol A in tea samples by solid phase extraction and liquid chromatography coupled to mass spectrometry, Microchem. J. 147 (2019) 598–604, https://doi.org/10.1016/j.microc.2019.03.026.
[11] N.C. Maragou, N.S. Thomaidis, G.A. Theodoridis, E.N. Lampi, M.A. Koupparis, Determination of bisphenol A in canned food by microwave assisted extraction, molecularly imprinted polymer-solid phase extraction and liquid chromatography-mass spectrometry, J. Chromatogr. B 1137 (2020) 121938, https://doi.org/10.1016/j.jchromb.2019.121938.
[12] T. Li, Y. Song, Z. Dong, Y. Shi, J. Fan, Hydrophobic deep eutectic solvents as extractants for the determination of bisphenols from food-contacted plastics by high performance liquid chromatography with fluorescence detection, J. Chromatogr. A 1621 (2020) 461087, https://doi.org/10.1016/j.chroma.2020.461087.
[13] D.O. Abranches, J.A. Coutinho, Everything you wanted to know about deep eutectic solvents but were afraid to be told, Ann. Rev. Chem. Biomol. Eng. 14 (1) (2023) 141–163, https://doi.org/10.1146/annurev-chembioeng-101121-085323.
[14] D.O. Abranches, J.A. Coutinho, Type V deep eutectic solvents: design and applications, Curr. Opin. Green Sustain. Chem. 35 (2022) 100612, https://doi.org/10.1016/j.cogsc.2022.100612.
[15] N. Fattahi, B. Hashemi, F. Shiri, M. Shamsipur, N. Babajani, Extraction of parabens from personal care products using a pH-responsive hydrophobic deep eutectic solvent: experimental design and COSMO-RS evaluations, N. J. Chem. 46 (33) (2022) 15851–15859, https://doi.org/10.1039/D2NJ02519A.

[16] M. Hassanpour, M. Shamsipur, N. Babajani, F. Shiri, B. Hashemi, N. Fattahi, pH-responsive deep eutectic solvents applied in the extraction of abamectin and endosulfan from water and fruit juice samples: a comparative study, Microchem. J. 187 (2023) 108391, https://doi.org/10.1016/j.microc.2023.108391.
[17] N. Fattahi, P. Zohrabi, F. Shiri, F.H.B. Sosa, B. Hashemi, Alcohol-based deep eutectic solvents with pH-responsive hydrophobicity for the analysis of herbicides in water and fruit juice samples, Sep. Purif. Technol. 339 (2024) 126607, https://doi.org/10.1016/j.seppur.2024.126607.
[18] N. Fattahi, B. Hashemi, P. Zohrabi, P. Karimi, F. Shiri, pH-switchable vortex-assisted liquid-liquid microextraction using hydrophobic eutectic solvents for the extraction of phthalate esters from water, fruit juice, and milk samples, Food Chem. (2025) 147208, https://doi.org/10.1016/j.foodchem.2025.147208.
[19] K.C. Ferreira, T. Rodrigues, G. Isquibola, S.C. Ayala-Durán, J. de Oliveira Merib, M. H. Gonzalez, J.L. Anderson, P.C.F. de Lima Gomes, Determination of parabens and bisphenol A in sludge samples using hydrophobic deep eutectic solvents by gas chromatography coupled to mass spectrometry and sample introduction via pyrolizer, Microchem. J. 207 (2024) 112057, https://doi.org/10.1016/j.microc.2024.112057.
[20] L. Cao, Y. Li, Synthesis and characterization of pH-responsive deep eutectic solvent followed by HPLC for trace determination of bisphenol A in water samples, J. Sep. Sci. 47 (1) (2024) 2300776, https://doi.org/10.1002/jssc.202300776.
[21] C. Steffen, K. Thomas, U. Huniar, A. Hellweg, O. Rubner, A. Schroer, TmoleX—A graphical user interface for TURBOMOLE, J. Comput. Chem. 31 (16) (2010) 2967–2970, https://doi.org/10.1002/jcc.21576.
[22] M. Frish, G. Trucks, H. Schlegel, G. Scuseria, M. Robb, J. Cheeseman, G. Scalmani, V. Barone, B. Mennucci, G. Paterson, Gaussian 09, Revision A. 02, Gaussian Inc, Wallingford CT, 2009.
[23] R. Bader, Atoms in Molecules: A Quantum Theory, Oxford University Press, Oxford, 1990.
[24] N. Fattahi, B. Hashemi, F. Shiri, M. Shamsipur, N.J.N. Babajani, Extraction of parabens from personal care products using a pH-responsive hydrophobic deep eutectic solvent: experimental design and COSMO-RS evaluations, 46(33) (2022) 15851–15859.
[25] K. Zhang, J. Wang, R. Guo, Q. Nie, G. Zhu, Acid induced dispersive liquid–liquid microextraction based on in situ formation of hydrophobic deep eutectic solvents for the extraction of bisphenol A and alkylphenols in water and beverage samples, Food Chem. 442 (2024) 138425, https://doi.org/10.1016/j.foodchem.2024.138425.
[26] M. Vargas-Muñoz, D. Montoya-Cárdenas, L. Bonilla, E. Palacio, Vortex-assisted binary solvent dispersive liquid–liquid microextraction for the determination of two 4-alkylphenols and bisphenol A in drinking water by HPLC-DAD, Microchem. J. (2025) 114167, https://doi.org/10.1016/j.microc.2025.114167.